

# Towards realization of a large-area light-emitting-diode-based solar simulator

B. H. Hamadani<sup>1</sup>, K. Chua<sup>2</sup>, J. Roller<sup>1</sup>, M. J. Bennahmias<sup>3</sup>, B. Campbell<sup>2</sup>, H. W. Yoon<sup>4</sup> and B. Dougherty<sup>1</sup>

<sup>1</sup>Engineering Laboratory, National Institute of Standards and Technology, Gaithersburg, MD 20899

<sup>2</sup>Physical Optics Corporation, Applied Technologies Division, Torrance, CA, 90501

<sup>3</sup>Bennahmias Consulting, Ladera Ranch, CA 92694

<sup>4</sup>Physical Measurements Laboratory, National Institute of Standards and Technology, Gaithersburg, MD 20899

## Abstract

Solar simulators based on light emitting diodes (LEDs) have shown great promise as alternative light sources for indoor testing of PV cells with certain characteristics that make them superior to the traditional solar simulators. However, large-area uniform illumination more suitable for larger cells and module measurements still remain a challenge today. In this paper, we discuss the development and fabrication of a scalable large-area LED-based solar simulator that consists of multiple tapered light guides. We demonstrate fine intermixing of many LED light rays and power delivery in the form of a synthesized air mass (AM) 1.5 spectrum over an area of 25 cm by 50 cm with better than 10 % spatial nonuniformity. We present the spectral output, the spatial uniformity and the temporal stability of the simulator in both the constant current mode and the pulsed-mode LED operation, and compare our data with the International Electrotechnical Commission (IEC) standards on solar simulators for class rating. Although the light intensity with our current design and settings falls short of the standard solar AM 1.5 intensity, this design and further improvements open up the possibility of achieving large-area, high-power indoor solar simulation with various desired spectra.

## 1. INTRODUCTION

Photovoltaic (PV) modules are rated based upon their maximum power output when subjected to a specific set of operating conditions. For convenience and cost, most PV manufacturers test and rate their products indoors using solar simulators. The key characteristics of the simulator used to perform the electrical performance measurements are its spectral output, its uniformity within the illumination

test plane, and its temporal stability when sweeping the test module's characteristic current versus voltage (IV) curve [1].

Current commercial-off-the-shelf (COTS) solar simulators, which typically use tungsten filaments or xenon (Xe) arc lamps as the illumination source, have limitations [2]. The lamp sources, for example, can only marginally approximate the spectral irradiance of a representative solar spectrum [3]. In addition, Xe lamps have strong multiple intensity spikes spanning from the ultraviolet (UV) to the near-infrared (NIR) [2]. In some solar simulators, spectral filters are used to modify the output of these lamps to better approximate specific solar conditions, but these filters cannot selectively suppress multiple intensity peaks from the Xe lamp nor simulate atmospheric absorptions by H<sub>2</sub>O, O<sub>2</sub>, O<sub>3</sub>, and CO<sub>2</sub> molecules. The deviation of the lamp's spectral output relative to that of a standard solar spectrum, and its effect of the module's IV measurement, can be compensated by determining a spectral mismatch factor for cases where the reference cell/module differs from the tested module [4,5].

Other deficiencies with COTS solar simulators include the variation of spectral irradiance from one simulator to another and the inability to easily vary the simulator's spectrum to simulate a realistic range of outdoor environmental conditions. Also, the simulator lamps are typically expensive, are not energy efficient (and so when operated in a steady-state mode will dissipate a large amount of thermal energy), and have emission characteristics that change over their relatively short  $\approx$  (150 to 1,000) h lifetimes [5, 7]. Finally, as solar modules become larger in size, the ability for COTS solar simulators to provide the needed performance levels is substantially challenged and more sophisticated simulators will be required to perform various measurement tasks [6]. Moreover, COTS simulators don't offer a means for incrementally increasing their application range to modules larger than those modules permitted as part of the original design. A solar simulator that can improve upon the above noted limitations is highly desirable.

Advancements in light emitting diodes (LEDs) over the last decade have contributed to an increase of their radiant emittance and spectral variety. With an increasing selection of available wavelengths, multiple LEDs of different wavelengths can be multiplexed and their outputs individually controlled so as to allow spectral simulation [7]. Additionally, LEDs have typical lifetimes that are at least an order of magnitude longer than conventional optical sources such as tungsten and xenon lamps. As a result of these advances and advantages, LEDs merit consideration as an alternative radiation source for solar simulators.

Recently, several groups have reported on the concept, design, and fabrication of an LED-based solar simulator and have shown both steady-state and flashed operations [7-12]. Two of these groups have demonstrated that with a limited, selected number of high powered LEDs at different central wavelengths mostly in the range of visible to near IR, 1 sun illumination intensity is achievable with class B uniformity over an area of 10 cm × 10 cm [7,8]. However, to achieve a larger illumination area with good uniformity and a better spectral match to air mass (AM) 1.5 spectrum, new LED simulator designs are required.

To this end, a scalable LED-based solar simulator that consists of multiple tapered light guides was designed and fabricated. The light guides are used to promote better mixing of the light rays and to yield more uniform power delivery over a larger area. Figure 1 depicts the components that are matched with each light guide of the prototype LED simulator design. Each simulator section consists of a matrix of water-cooled LEDs, multiple computer-controlled LED drivers, and a 5 m long tapered light guide. The LED matrix is populated with an optimum number of LED chips of different wavelengths. The LED chip density is maximized by eliminating the footprints associated with typical LED packaging. Each LED matrix consists of 34 high-power LEDs of different wavelengths (See Table 1 below), and are all mounted on a water-cooled substrate. Computer-controlled LED drivers, each capable of independently

controlling four LEDs, regulate the current supplied to each LED within the matrix. These current levels are adjusted to create a tuned combined output spectrum as described under the experimental section.

Each LED matrix is positioned at the small end of a light guide. The guide is tapered to improve the uniformity of the combined emittance outputs from all the LEDs while allowing the smaller source to irradiate a larger test area. A ray tracing software simulation program was used to verify the effectiveness of the tapered feature for improving the blended output uniformity.

The following sections discuss the light guide design and simulation, the light guide fabrication, and the characterization of the system's performance. Conclusions and proposed options for future improvements are offered.

## **2. TECHNICAL DESCRIPTION**

### **2.1. Tapered Light Guide**

The tapered light guide performs two functions: (1) creating a uniform irradiance from an extended source of multiple, high powered LEDs, and (2) permits multiplexing of sources having different wavelength bands. The light guide length and ratio of the input-to-output apertures were optimized so that the output irradiance will meet a certain uniformity tolerance. The light tracing program ZEMAX [13] was used for developing an initial light guide design, where we modeled a 3 meter-long light guide with an input aperture of 7.6 cm × 7.6 cm and output aperture of 30.5 cm × 30.5 cm. The optical layout for the ray-tracing simulation of the 3-m-long tapered light guide is shown in Figure 2.

As part of the simulation, a virtual detector, with dimensions 30.6 cm by 30.6 cm and pixel counts 305 by 306 for width and height respectively, was placed at the exit aperture of the simulated mirror waveguide. The detector was used to evaluate the degree of mixing generated by different LED array geometries. A 6 × 6 array of LEDs is shown in Figure 3. Approximately 200 000 optical rays were

launched from each LED to more accurately track the energy loss. It was determined that 36 LEDs would provide sufficient spectral content in the illumination to simulate the AM 1.5 spectrum between the wavelengths of 400 nm to 970 nm.

The typical radiant intensity of a modeled single LED source is shown in Figure 4a. The emission half-angle,  $\theta_{1/2}$  according to the manufacturer's specifications, is  $60^\circ$ . Note that the average irradiance at the output surface is  $100 \text{ mW/cm}^2$ . After propagating through the 3 m-long tapered light guide and undergoing multiple reflections, the output angle for the exit illumination is reduced to  $12^\circ$ , as shown by the calculated radiant intensity pattern at the output aperture shown in Figure 4b. The difference in angular profile is in good agreement with the conservation of the brightness theorem (i.e., the second law of thermodynamics):

$$B_1 A_1 \pi \sin^2(\theta_1) = B_2 A_2 \pi \sin^2(\theta_2) \quad (1)$$

Where  $A_1$  and  $A_2$  are the input and exit plane areas,  $B_1$  and  $B_2$  are parameters related to absorption of light in the propagating media, and  $\theta_1$  and  $\theta_2$  are the half-angles at the entrance and the exit planes, respectively. Since the area of the output face is 16 times larger than the input face (and assuming no absorption in the reflective coating of the mirror so  $B_1 \approx B_2$ ), the sine of the half-angle of the output illumination must be 1/4 the input half-angle from the LED ( $\approx 12.5^\circ$ )—which is clearly the case.

The illumination uniformity at the output aperture of the light guide, as “measured” by the virtual detector, is shown in Figure 5a. To quantify the uniformity of the illumination profile, a row cross section of the incoherent irradiance profile at the output face was examined, as shown in Figure 5b. This evaluation shows a nonuniformity of  $< 2\%$  root mean square (RMS) over a distance of about 28 cm.

Based on the simulation results, a decision was made to fabricate four 5 m long light guides for even better light mixing. Each light guide is made of highly reflective aluminum sheets (Miro-Silver 2AG

from Alanod) [13] with reflectivity of 98 % from  $\approx 500$  nm to  $\approx 750$  nm wavelengths. The guide's input and output apertures are  $7.6 \text{ cm} \times 7.6 \text{ cm}$  and  $30.5 \text{ cm} \times 30.5 \text{ cm}$ , respectively. The four light guides are mounted on an adjustable steel support structure in a  $2 \times 2$  configuration. The support structure allows the separation between each light guide to be adjustable by 2.5 cm increments.

The easiest and most rigid construction of the light guide using the aluminum panels is with bolts securing the panels together. However, bolts protruding inside the light guide would cause artifacts and ruin the reflectance of the interior surfaces. To prevent this, four spines were assembled from right-angle aluminum stock and bolted together. Using right-angle joints allows the protruding adjacent legs to be bolted together easily, while the other protruding legs give flat surfaces for the mirrored aluminum to contact the spines. The mirrored panels were epoxied into place, and bolt holes were added to the spines to allow brackets to be fitted on all sides to secure the guides into the mounting racks. The epoxy also has the same coefficient of expansion as the aluminum sheeting and spine pieces, so temperature changes do not distort the thin aluminum panels which could cause reflectance artifacts. The assembled light guides are shown in Figure 6.

## **2.2 LED Matrix**

To construct a LED-based solar simulator, high-powered LEDs are desired. Some LED manufacturers offer very high power LEDs (15 W), but only with few available wavelengths, typically ultraviolet (405 nm), green (518 nm), amber (590 nm), red (627 nm), and white (5500 K). While useful, these select few colors will not produce the shape of the AM 1.5 spectrum. In order to fill the missing spectra gaps, LEDs at other wavelengths but having weaker outputs were purchased and used. Each LED is composed of 60 diode dies mounted on a metal and ceramic heat sink and covered with a double coated clear silicone and epoxy resin lens for wide viewing angle. The LED chip is circular and is roughly 11 mm in diameter. Excess footprint of the LED's package was milled off to allow more LED packages

mounted per unit area. These LEDs were mounted on a square water-chilled aluminum heat sink that is about 8.9 cm × 8.9 cm as shown in Figure 7. On this plate, 30 of the lower-powered LEDs were mounted, along with 4 high power LEDs (2 whites, 1 violet and 1 green), that were mounted near the top edge. All the LEDs are powered by USB controlled LED drivers. Each of these current drivers can drive 4 LEDs, and is fully addressable by a software development kit (SDK) to aid in custom software programming.

To allow the user to easily adjust many LED drive currents at any given time, a custom graphic user interface (GUI) was developed to control the LED drivers. The software uses profile files that can be created and loaded by the user to quickly load a predefined current profile to drive the LEDs to create a certain spectral output. The current of each diode can be controlled to the milliamp level over a range of 0 to 1000 mA. The software permits the LED matrixes to be operated in a constant mode and in a pulsed mode.

### **3. EXPERIMENTAL TESTING**

One of our main objectives of this project was to demonstrate good light mixing and large area uniform illumination with a closely synthesized AM 1.5 spectral irradiance. To this end, each plate was designed and fabricated with the same set of LEDs of many different wavelength varieties to give ultimate flexibility in control of the irradiance spectrum. The first three columns in Table 1 show the 34 selected LEDs with their rated wavelength and current limits. The LEDs are named in the format *x.y*, where *x* is the LED driver number, and *y* is the LED channel number. Each driver has 4 current source channels as mentioned previously.

To gain an initial understanding for the potential output range of the LED matrix, a NIST calibrated spectroradiometer [1] was used to measure the irradiance of each individual LED. For these measurements, the integrating sphere of the spectroradiometer was positioned at the center of the light guide exit plane. Each individual LED was operated close to its rated current limit in constant

mode. Columns (4 and 5) of the table show the measured wavelength (central peak) and the spectral emission width in terms of full width at half max (FWHM) as determined by a Gaussian fit to each emission profile. The difference between the manufacturer-rated emission wavelength and the measured value are observed to be 13 nm or less. These comparisons and the approach taken by the manufacturer to report the wavelengths mostly in 5 nm increments provides guidance as to the extent that an individual LED may depart from the manufacturer's nominal rating. With regard to their spectral width, the chosen LEDs yielded values that varied from 33 nm at  $\lambda=515$  nm, to 13 nm at  $\lambda=572$  nm, to 46 nm at  $\lambda=971$  nm. Therefore, it is important to perform these measurements on all LEDs prior to their use in a measurement scheme.

Column 6 of table 1 shows the total irradiance of each LED in  $\text{W}/\text{m}^2$  as determined by integration of the spectral profile with respect to wavelength. Because these measurements were performed at the exit plane of the LED light guide, the irradiance is much lower than if the measurement had been made over a smaller solid angle in close proximity to the LED source. It is clearly seen that certain LED colors provide very weak outputs, especially in some regions of the ultraviolet-visible (UV-VIS) spectrum, while the majority of the near infrared (NIR) LEDs have higher power outputs. This means that in order to achieve a balanced AM 1.5 spectrum, more UV-VIS LEDs are required than NIR ones.

In Figure 8a, we show the synthesized AM 1.5 spectrum based on one LED plate illuminating into one of the light guides in constant DC current mode (straight line). The irradiance levels and the total intensity are clearly very low compared to the intensity of  $1000 \text{ W}/\text{m}^2$  used for rating solar modules; however, via precise control over the electrical current supplied to each LED chip, and with the large number of available wavelengths, a good match to the shape of the solar spectrum can be achieved. This matching is demonstrated well in Fig 8b by plotting 535 nm-normalized global AM 1.5 and our synthesized spectra on the same graph. The extent of the spectral match of the simulator to the AM 1.5

reference spectrum is evaluated by the guidelines in the IEC Standard 60904-9 [14]. For the overall interval of (400 to 1100) nm, the percentage of total irradiance in each of the six wavelength sub intervals is calculated. Based on the ratio of the measured simulator irradiance percentage to the IEC standard percentage for each spectral sub interval, a class rating is assigned. Table 2 shows these ratios and subsequent class ratings for the LED simulator. For the spectral bands covering 400 nm to 900 nm, a mix of A and B ratings is achieved. The B ratings, moreover, are mostly on the borderline of A/B rating and so can be converted to an A rating with further fine-tuning. The final band between 900 nm to 1100 nm achieves a C rating which can be improved by the addition of infrared (IR) LEDs with emission wavelengths greater than 1000 nm.

The data plots shown in Figure 8 were obtained with the LED heat sink plate maintained at a temperature of 15 °C. However, we note that the emission characteristics of LEDs can change with the temperature of the environment. Figure 9 shows a series of irradiance curves collected at several plate temperatures ranging from 10 °C to 37 °C, revealing a small deterioration in the emission intensity for visible range LEDs, but a larger drop in the peak maxima for IR LEDs. We also observe a small shift in the center peak wavelength towards higher wavelengths values, particularly for the IR LEDs. These results indicate that it is important to maintain an isothermal heat sink contact to the mounted LEDs and preferably operate at temperatures below 20 °C to obtain optimal emission from the LEDs and avoid intensity fluctuations due to the changes in the temperature of the environment.

In order to achieve higher intensities, the LEDs can be operated in a pulse mode using higher currents. Some LEDs, particularly those in the UV and low VIS range, can be pulsed with a current up to 2 times the constant mode current. The majority of the red and near infra-red (NIR) LEDs, can be pulsed with a current up to a factor of 5 times higher than recommended for constant mode operation. In Figure 8a, the dashed line shows the irradiance as a function of wavelength for all the LEDs of one plate,

all triggered simultaneously by a function generator providing a pulse duration of 50 ms at a frequency of 1 Hz. Although much higher powers are achievable, current levels double the amounts used for the constant-current operation were selected in an effort to preserve the overall shape of the AM 1.5 synthesized spectrum. That's because the LEDs for the range of 400 nm to 600 nm were not bright enough to match the higher power IR ones. By using this pulse mode of operation, the intensity was increased from 28.9 W/m<sup>2</sup> to 52.3 W/m<sup>2</sup>.

The temporal stability during both the constant current and the pulse mode operations was also examined. The inset in figure 10 shows the monitored intensity of our LED simulator output in constant current mode as a function of time after the LEDs were initially turned on and allowed to reach steady operation. This particular data set was taken approximately 15 min after the LEDs had been turned on. The temporal stability, which is defined as the approximate range from the mean, was found to be within  $\pm 0.6\%$ . In accordance to the criteria for temporal instability as specified in IEC Standard 60904-9, this level of performance earns the LED simulator a Class A rating. The main part of Figure 10 shows the simulator's normalized irradiance in pulse mode over a period of 50 ms, as measured by a fast photodiode. The pulse has very fast rise and fall times ( $< 100\ \mu\text{s}$ ) with a temporal stability of  $\pm 1.2\%$ , translating to a class A rating under IEC standards.

The spatial uniformity of the irradiance from the LED solar simulator was evaluated at the exit plane of the light guides and at 34 cm spacing from the exit plane. The measurements reported here are taken for 2 of the 4 light guides. Figures 11a and 11b show the total irradiance map at the immediate exit plane of two vertically adjacent light guides. The map is constructed by taking an irradiance measurement at a series of 3-cm distance intervals in both the X and Y directions using a calibrated spectroradiometers. The spectroradiometer's integrating sphere has an input collection aperture of 1

cm in diameter. Each irradiance plot as a function of wavelength is integrated with respect to  $\lambda$  to provide the total irradiance at a given X-Y coordinate.

Figure 11a reveals a 9.7 % irradiance nonuniformity (calculated according to the IEC Standard 60904-9, by taking the ratio of (Max irradiance – Min irradiance)/(Max irradiance + Min irradiance)) over an area of 27 cm by 27 cm (excluding the small region near the bottom right edge) thus qualifying it as a Class C solar simulator. Within a 15 cm by 15 cm sub area, the nonuniformity was reduced to approximately 4 %, which equates to a Class B simulator rating. As for the second light guide, figure 11b reveals a 5.6 % irradiance nonuniformity over the 27 cm by 27 cm exit plane (excluding the small region near the top left edge), thus again qualifying as a Class C solar simulator. This second LED matrix and light guide also exhibited better performance for a sub area: for a 10 cm by 10 cm area the nonuniformity was limited to approximately 3 percent, good enough for a Class B rating.

Figure 11c shows the irradiance uniformity map of the two combined light guides during simultaneous operation at a distance of 34 cm away from the exit plane. As the light spreads over a larger area, the overall intensities drop by a small amount (about 4 W/m<sup>2</sup>). Also, the light fills the gap between the two light guides, allowing for a near seamless overall illumination area with less than 10 % nonuniformity over an area of 25 cm by 50 cm. In figure 12, we show the spatial uniformity of different spectral components. Figure 12a shows the spatial distribution of the total intensity over all wavelengths for one of the light guides a distance of 34 cm from the exit plane, with similar uniformity as discussed above. In figures 12b-12f, we show the integrated irradiance for spectral bands of 400 nm-500 nm, 500 nm-600 nm, 600 nm-700 nm, 700 nm-800 nm, and 800 nm-1000 nm, respectively. There are variations in the power distribution for each spectral band with more noticeable “hot” or “cold” spots for certain bands such as the 500 nm to 600 nm spectral region. The spatial nonuniformity increases to up to 15 % for some of these bands over an extent of 25 cm, but the overall spectral

nonuniformity as indicated in Figure 12a remains below 10 %. Below, we discuss ways to improve the spatial uniformity of the illuminated output plane.

#### **4. FURTHER DISCUSSIONS**

The experimental results of the irradiance uniformity at the output of the light guides do not exactly follow the predictions of the light tracing simulations. Specifically, certain hot (higher irradiance) or cold (lower irradiance) regions are observed across the exit plane, thus indicating locations where an effective mixing of LED colors did not occur. The origin of these small-area nonuniformities was not determined, but the results suggest that a mirror-like interior surface and the use of specular reflection to achieve light mixing is subject to imperfections, and is not likely to produce a class A simulator for spatial uniformity. We envision several ways to improve the spatial uniformity, while reducing the extensive footprint of such a system. As the LED fabrication technology matures, it may be possible to custom-fabricate LED chips that incorporate many die colors within one package in much closer proximity (tens of microns) to each other than the current individually-mounted design (millimeters). This will result in much finer color mixing over smaller areas. Additionally, we believe incorporation of suitable micro lens arrays over each individual LED, the whole plate of LEDs or at intervals inside the light guide should result in improved light mixing and better spatial uniformity, although we were unable to test this with our current apparatus design and its restrictions. Finally, replacing the interior mirror-like coating with a diffusive coating such as those incorporated inside integrating spheres should provide better light mixing and uniformity. Successful implementation of these approaches to improve light mixing and uniformity should in principle allow for a reduction in the total size of the light guide.

Although we acknowledge that the addressed deficiencies of the current system and the large physical space required to maintain and operate it may be viewed as a deterrent to its implementation in academic or industrial research facilities, this system has been evaluated and discussed here primarily

as a prototype experimental approach to test the viability of a large-area LED based solar simulator. With improvements in design and use of higher power LEDs as they become available in the market, it should be possible to enhance the performance characteristics of this solar simulator. Furthermore, efforts are currently under way to also utilize this system and the pulsing capability of each LED to perform spectral response measurements on small or large solar cells in the presence of light bias. The results of these experiments will be discussed in a forthcoming publication.

## **5. CONCLUSIONS**

An investigation into the design and performance of an LED solar simulator has been completed. Using LEDs of different emission profiles, a near continuous broad band spectral illumination source can be created. Through independent and precise control of the current supplied to each LED, a synthesized spectrum having an the overall relative shape that approximates that of an AM 1.5 spectrum was achieved for the interval of 400 nm to 970 nm. The LED solar simulator design generated an irradiance where the nonuniformities didn't exceed 10 % over an area of 25 cm by 50 cm.

Advancements in the LED technology should allow for extending the spectral range below 400 nm into the UV region and beyond 1000 nm into the NIR range. Although the intensity of the produced spectrum at the output plane of the light guide is currently low, work is under way to increase the delivered optical power by utilizing several LEDs of each wavelength for each plate. In pulsed mode, more current may be supplied to each LED, resulting in a significant increase in the total irradiance. With increased optical output power, and given the results outlined in this paper regarding the temporal stability, spectral uniformity and spatial uniformity of illumination over large areas, the LED based solar simulators should challenge for commercialization in the near future.

## **Acknowledgements**

We would like to thank Nikolai Zhitenev of NIST for useful discussions, Tomasz Johnson of POC for the idea of using tapered light guides for this project, Robert Kunc of POC for programming and controls of the LED drivers, and William Healy and Hunter Fanney of NIST's Engineering Laboratory for their continuous feedback, support and encouragements leading to completion of this work.

## References

- [1] IEC Standard 60904-9, "Photovoltaic Devices-Part 9: Solar simulator performance requirements" *International Electrotechnical Commission*, Edition 2.0, 2007.
- [2] Yoon HW, Dougherty BP, Khromchenko VB. Spectroradiometric characterization of the NIST pulsed solar simulator. *Proc of SPIE* 2009; **7410**.
- [3] ASTM Standard G 173 – 03, "Standard Tables for Reference Solar Spectral Irradiances: Direct Normal and Hemispherical on 37° Tilted Surface" *ASTM International*. [www.astm.org](http://www.astm.org)
- [4] IEC Standard 60904-7, "Photovoltaic Devices-Part 7: Computation of spectral mismatch error introduced in the testing of a photovoltaic device" *International Electrotechnical Commission*, Edition 3, 2008.
- [5] Emery K. Photovoltaic efficiency measurements. *Proc. SPIE* 2004; **5520**: 36-44.
- [6] Zettl M, Stern O, Mayer O, Hartung M, Lynass M, Bernal E. Indoor characterization of photovoltaic modules under various conditions. *Proc of SPIE* 2008; **7056**: 70460M.
- [7] Krebs FC, Sylvester-Hvid KO, Jorgensen M. A self-calibrating led-based solar test platform. *Prog. Photovolt: Res. Appl.* 2011; **19**(1): 97-112.
- [8] Bliss M, Betts TR, Gottschalg R. An led-based photovoltaic measurement system with variable spectrum and flash speed. *Solar Energy Materials and Solar Cells* 2009; **93**: 825-830.
- [9] Kohraku S, Kurokawa K. A fundamental experiment for discrete-wavelength led solar simulator. *Solar Energy Materials and Solar Cells* 2006; **90**: 3365-3370.
- [10] Yuki T, Kamisako K, Kosuke K. New generation of PV module rating by LED solar simulator - A novel approach and its capabilities. *Photovoltaic Specialists Conf.* 2008; **492582**: 1-5.
- [11] Young DL, Pinegar S, Stradins P. New Real-Time Quantum Efficiency Measurement System. *33<sup>rd</sup> IEEE Photovoltaic Specialists Conference*, San Diego, California, 11–16 May, 2008.
- [12] Grischke R, Schmidt J, Albert H, Laux A, Metz A, Hilsenberg U, Gentischer J. Led flasher arrays (lfa) for an improved quality control in solar cell production lines. In *European Photovoltaic Solar Energy Conference*, 2004; **2**, 2591-2594.
- [13] Certain equipment, instruments, or materials are identified in this paper in order to adequately specify the experimental details. Such identification neither implies recommendation by the National Institute of Standards and Technology nor does it imply the materials are necessarily the best available for the purpose.

## Figure Captions

Figure 1: Block diagram of the scalable LED-based solar simulator.

Figure 2: Ray-tracing simulation of the 3-m-long tapered light guide.

Figure 3: LED matrix used in the simulation. It consists of 34 high powered LEDs of different wavelengths. The array has dimensions of 78 mm X 78 mm.

Figure 4: (a) Radiant intensity of a typical LED. (b) Simulated radiant intensity pattern at the output aperture of the light guide. For these figures, both the x and y dimensions range from  $-90^\circ$  to  $90^\circ$ .

Figure 5: (a) Simulation intensity profile at the output aperture. The dimensions are 30.6 cm by 30.6 cm (b) A line cross section of the simulated illumination profile at the output aperture near the center.

Figure 6: Assembled light guides using front surface reflecting MiroSilver 2AG from Alanod [13]. It has four 5-m-long light guides, each with an input and output aperture of 7.6 cm  $\times$  7.6 cm and 30.5 cm  $\times$  30.5 cm, respectively.

Figure 7: (a) LED matrix heat sink/mount with built-in water circulating channels. (b) The same LED plate in operation under a small current to each LED. The LEDs on the second row from the bottom emit most of their radiation in the NIR region (Table 1, LEDs 5-3 to 6.4) and hence appear very faint to the human eye. The bottom row LEDs (LEDs 7.1 to 8.2) are completely invisible to human eye.

Figure 8: (a) The synthesized AM 1.5 spectrum from a combination of LEDs listed in Table 1 as measured at the exit plane of one of the light guides in steady state current mode (solid line) and under pulsed operation (dash line) with higher applied currents. (b) The normalized LED synthesized spectrum as

compared with the normalized AM 1.5 Global irradiance spectrum. Both plots are normalized to 1 at  $\lambda = 535 \text{ nm}$ .

Figure 9: The dependence of the LED irradiance on the heat sink plate temperature. At higher temperatures of the coolant fluid that circulates through the plate, all LEDs show degradation in total irradiance with the effect most severe for IR LEDs.

Figure 10: (inset) Monitored intensity of the LED simulator output in constant current mode as a function of time. (main) The simulator operation in pulse mode over a period of 50 ms, as measured by a fast photodiode, showing a fast rise time with a temporal stability of  $\pm 1.2 \%$ .

Figure 11: (a) and (b) The irradiance uniformity contour maps at the immediate exit planes of two light guides mounted next to each other. (c) The 3-D irradiance uniformity map of the two combined light guides during simultaneous operation at a distance of 34 cm away from the exit plane showing less than 10 % nonuniformity in illumination over an area of 25 cm by 50 cm.

Figure 12: (a) The total irradiance uniformity contour map for one light guide at a 34 cm distance from the exit plane. (b-f) The irradiance uniformity maps for the different spectral components of the light as marked on the graphs.

### **Table captions**

Table 1: The characteristics of all the LEDs used on each plate. The manufacturer's rated wavelengths are oftentimes different from the measured emission of the LEDs. Here, we determined the central emission peak and the FWHM of each LED by performing a Gaussian fit to the irradiance response. The uncertainty in the measured  $\lambda$  and FWHM values is 1 nm. The uncertainty of the measured total irradiance is around 0.01 W/m<sup>2</sup>. The total integrated irradiance of each LED is determined by integrating the area under each emission peak.

Table 2: The irradiances at the spectral bands as specified by the IEC Standard 60904-9.

Table 1

LED no	Rated $\lambda$ [nm]	Rated I [mA]	Measured $\lambda$ [nm]	Measured FWHM [nm]	Measured total irradiance [ $w/m^2$ ]
1.1	395	240	400	14	0.74
1.2	420	240	408	19	0.48
1.3	450	240	448	22	0.83
1.4	470	240	461	23	1.28
2.1	505	240	515	33	0.64
2.2	525	240	515	33	0.55
2.3	565	240	568	24	0.04
2.4	570	240	572	13	0.20
3.1	590	240	589	15	0.50
3.2	620	240	613	18	0.74
3.3	630	240	627	16	2.30
3.4	645	240	634	16	1.93
4.1	660	240	651	21	0.69
4.2	670	240	669	23	1.89
4.3	680	240	680	23	0.95
4.4	690	240	678	22	1.14
5.1	700	240	689	24	1.26

LED no	Rated $\lambda$ [nm]	Rated I [mA]	Measured $\lambda$ [nm]	Measured FWHM [nm]	Measured total irradiance [ $w/m^2$ ]
5.2	735	600	733	28	4.01
5.3	750	600	749	28	3.84
5.4	760	600	756	28	4.87
6.1	780	600	777	29	4.14
6.2	790	600	781	33	3.88
6.3	810	600	810	30	4.59
6.4	830	600	825	31	3.16
7.1	850	800	844	42	6.27
7.2	870	800	861	44	5.53
7.3	890	800	883	48	2.32
7.4	910	800	897	38	2.21
8.1	940	800	937	65	2.60
8.2	970	800	971	46	0.61
9.1	W	1000	--	--	8.87
9.2	W	1000	--	--	8.25
9.3	518	1000	517	44	4.20
9.4	405	700	407	17	3.92

Table 2

Beginning Wavelength [nm]	Ending Wavelength [nm]	Integrated Irradiance [W m <sup>-2</sup> ]	Measured Percentages	IEC Standard Percentages	IEC Ratio	Class Rating
400	500	3.89	13.6 %	18.4 %	0.74	B
500	600	6.99	24.4 %	19.9 %	1.23	A
600	700	7.01	24.5 %	18.4 %	1.33	B
700	800	3.86	13.5 %	14.9 %	0.90	A
800	900	4.59	16.0 %	12.5 %	1.28	B
900	1100	2.30	8.03 %	15.9 %	0.51	C
	Total	28.64				

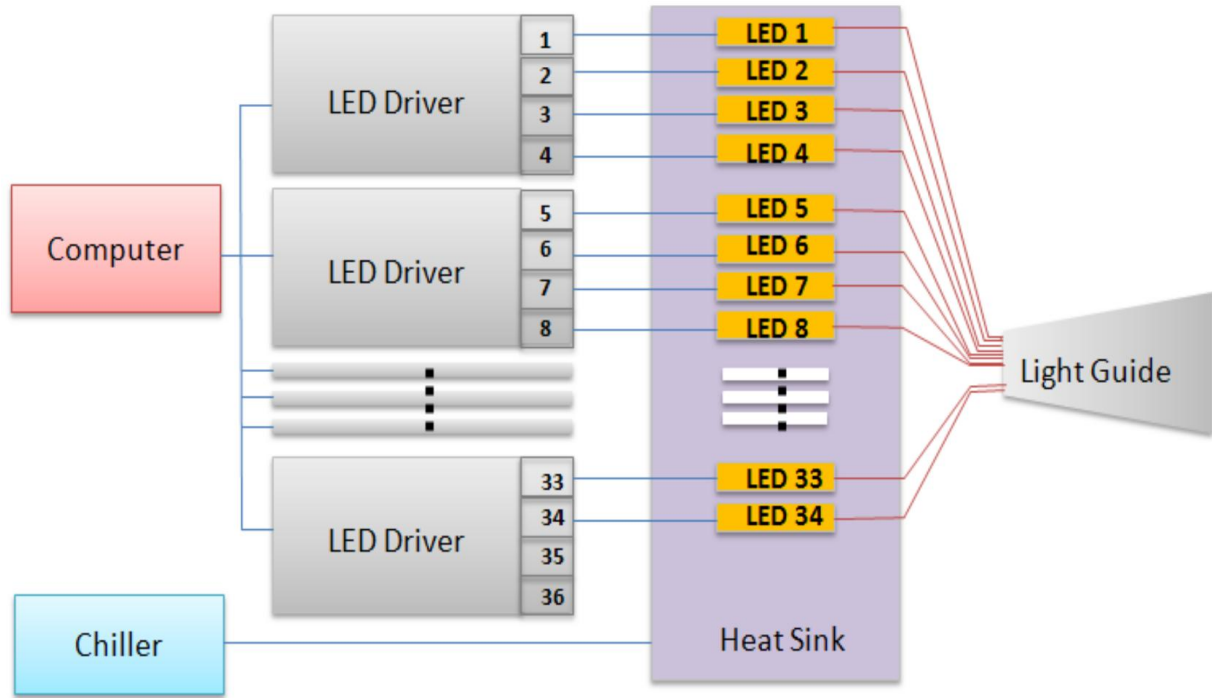
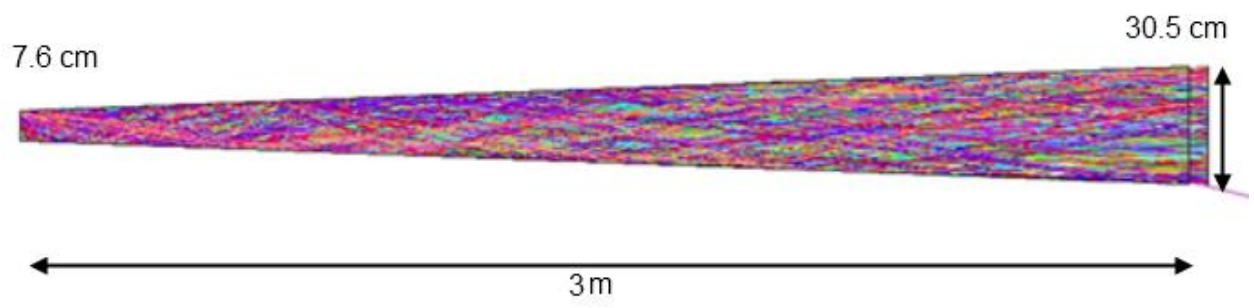


Figure 1



L.

Figure 2

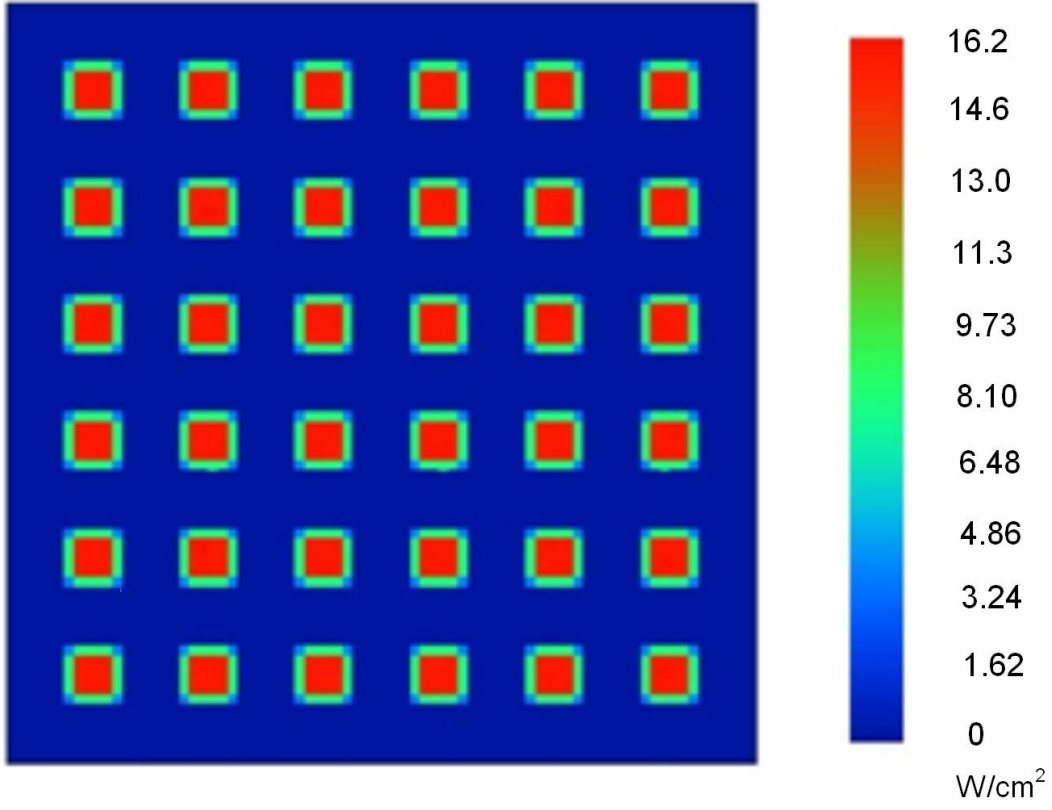


Figure 3

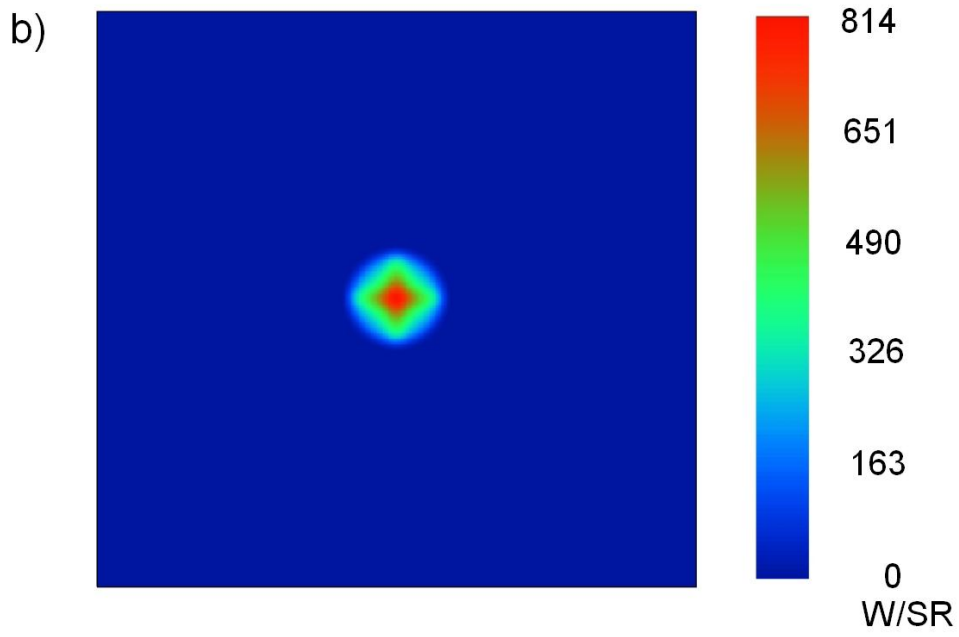
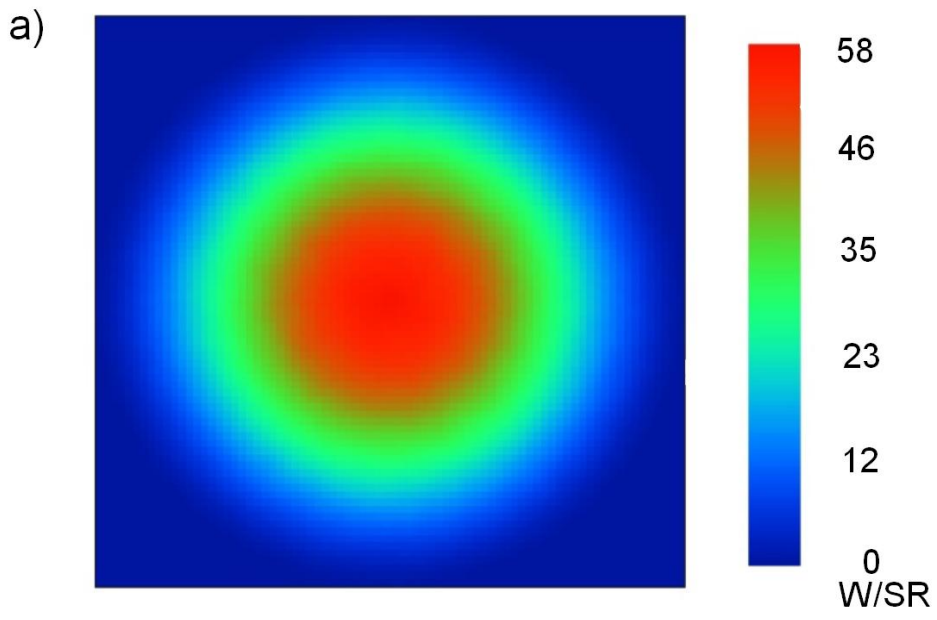


Figure 4

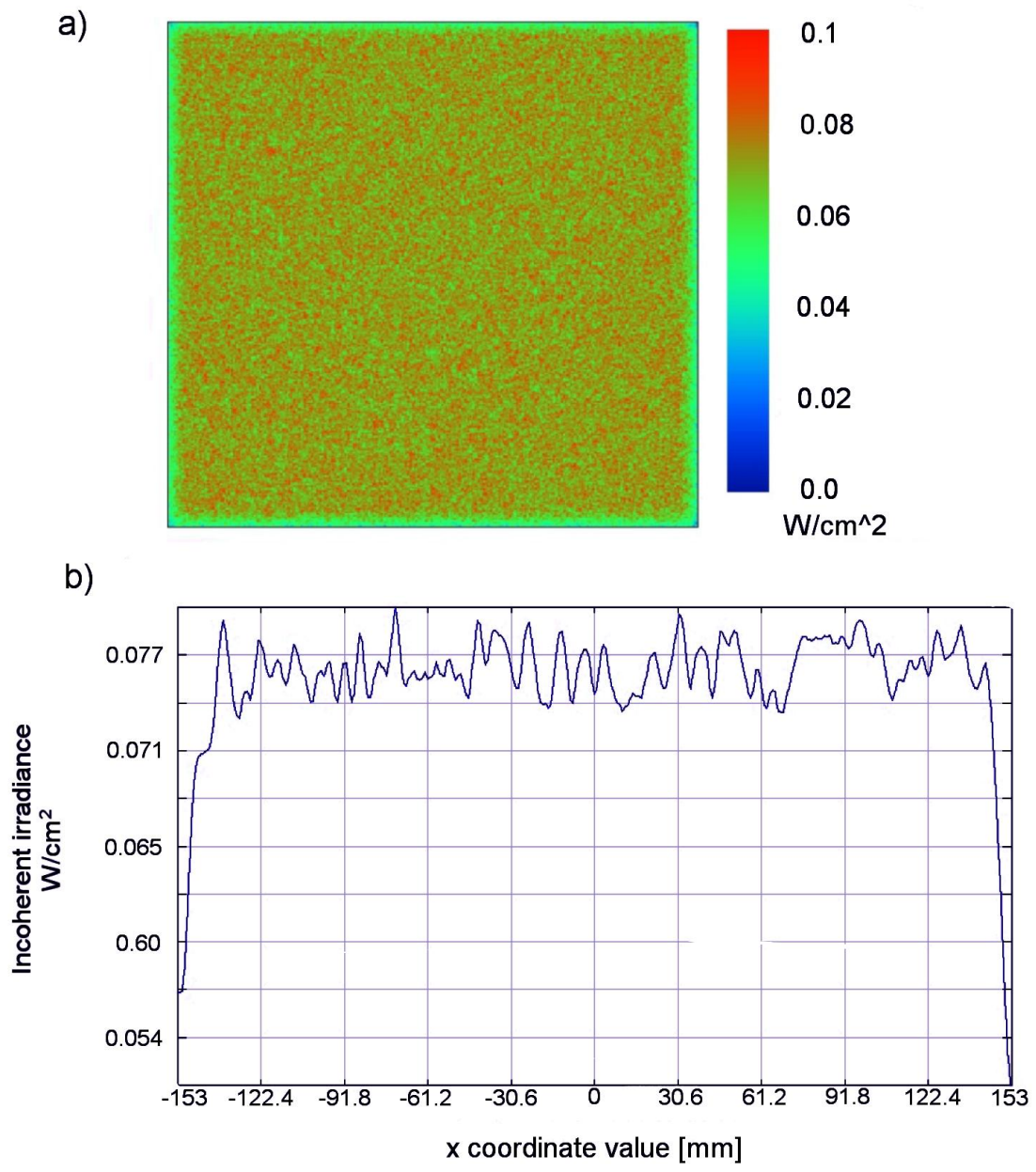


Figure 5



Figure 6

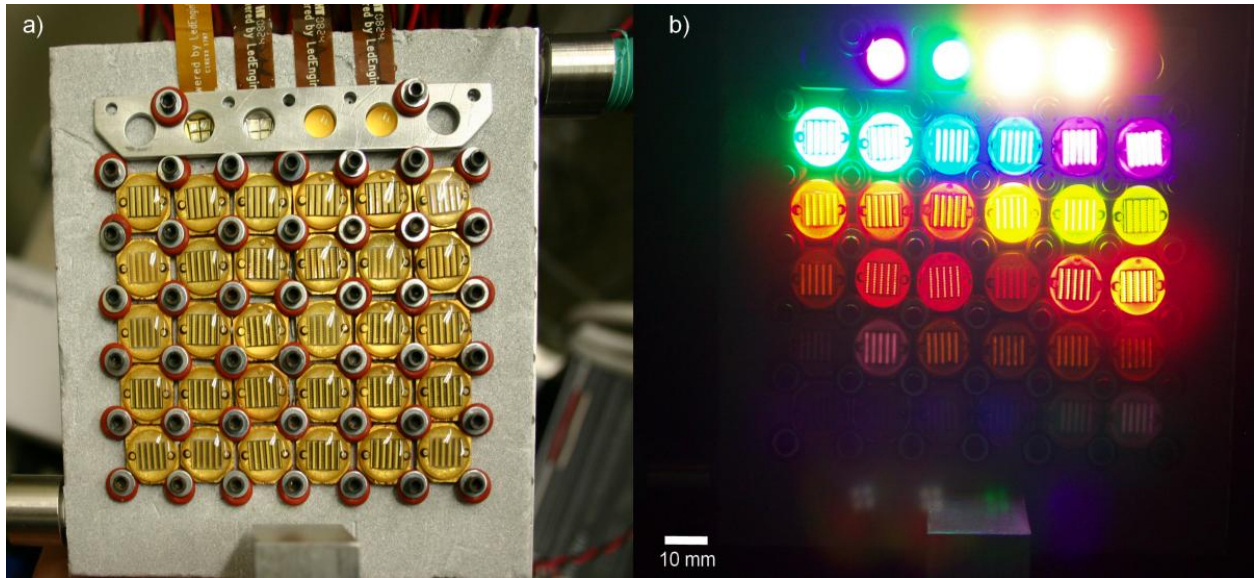


Figure 7

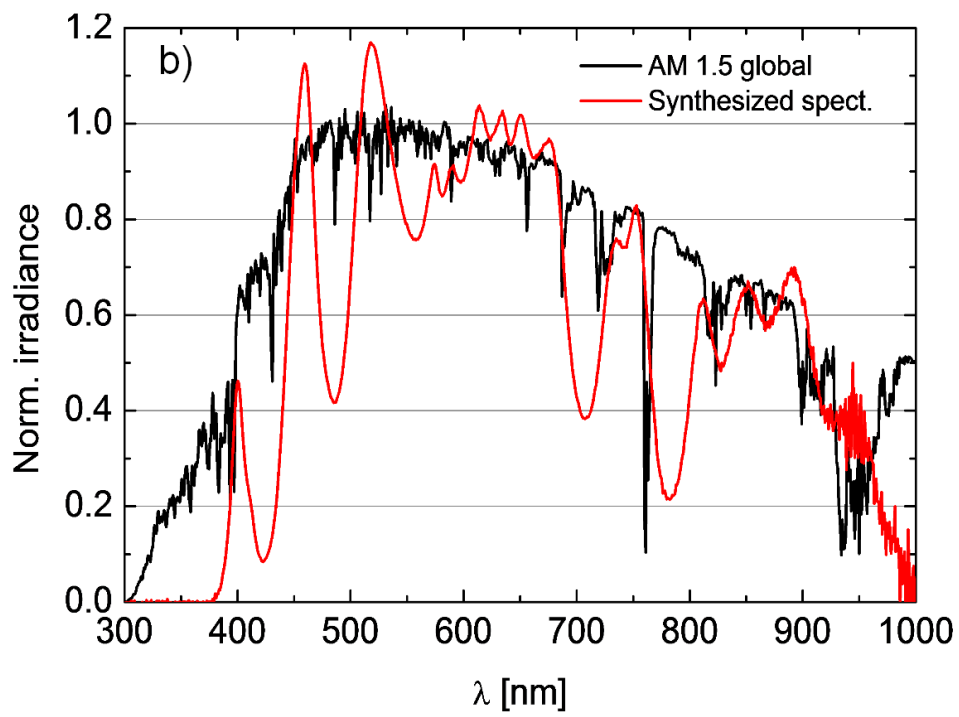
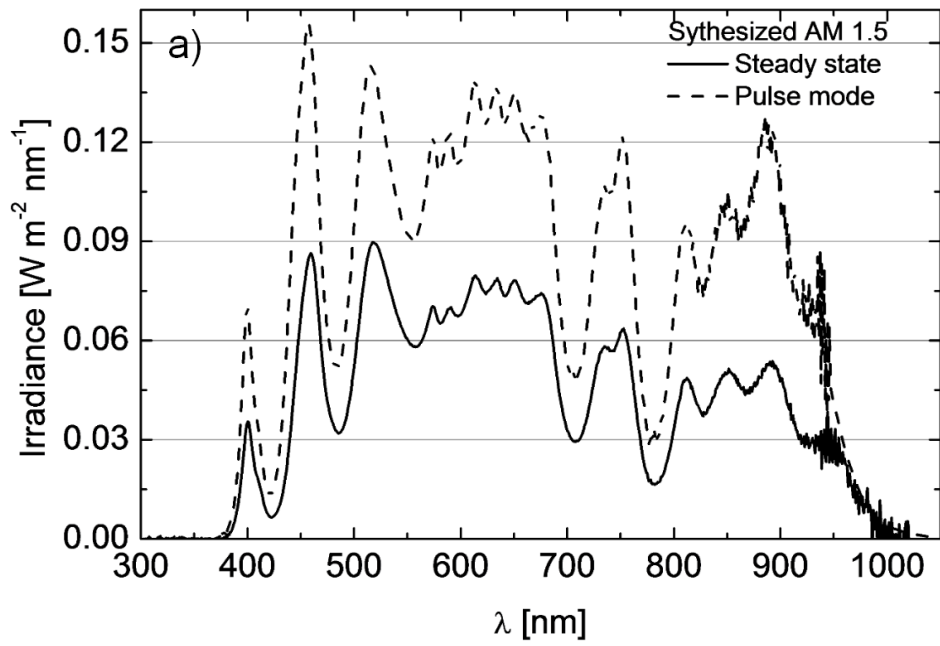


Figure 8

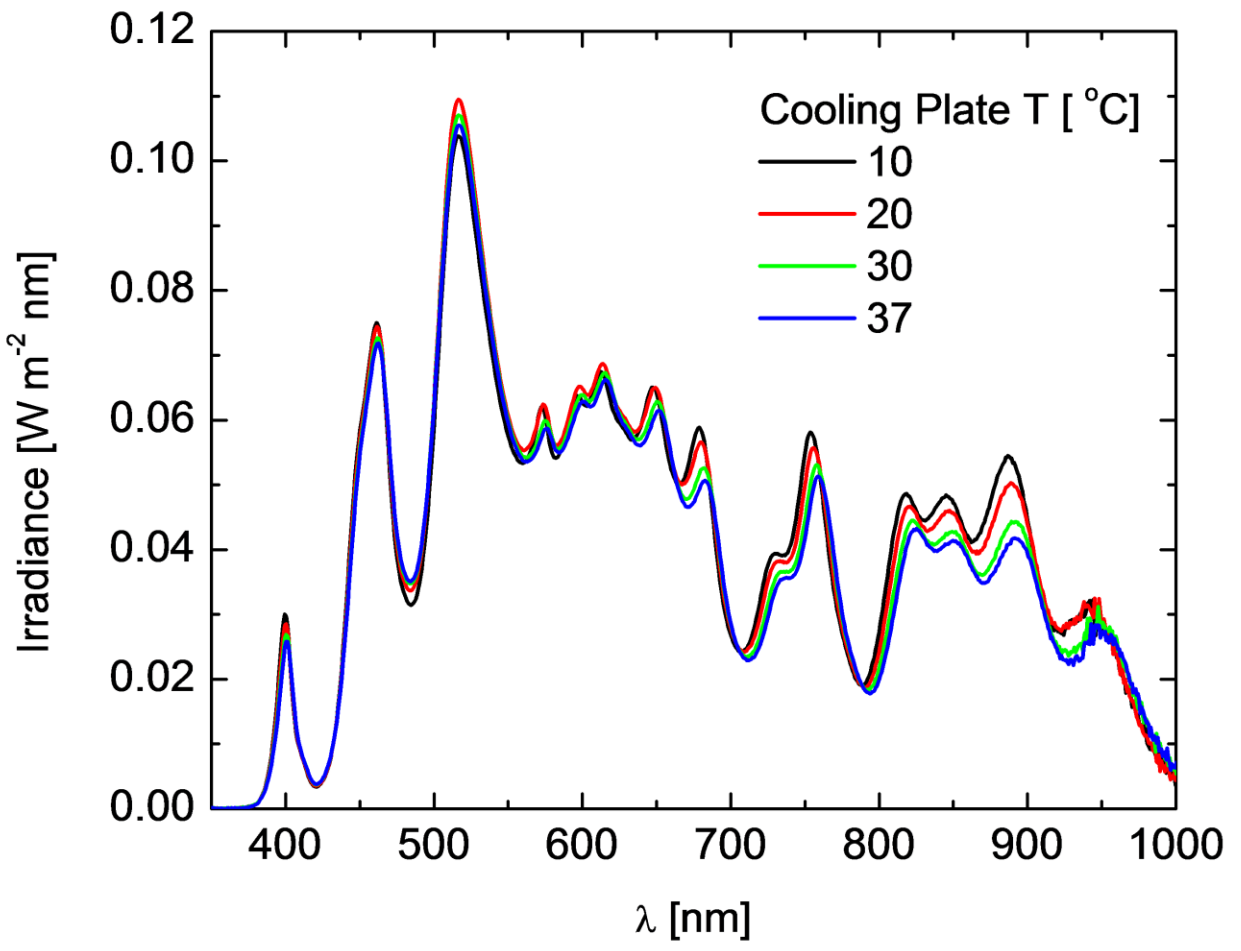


Figure 9

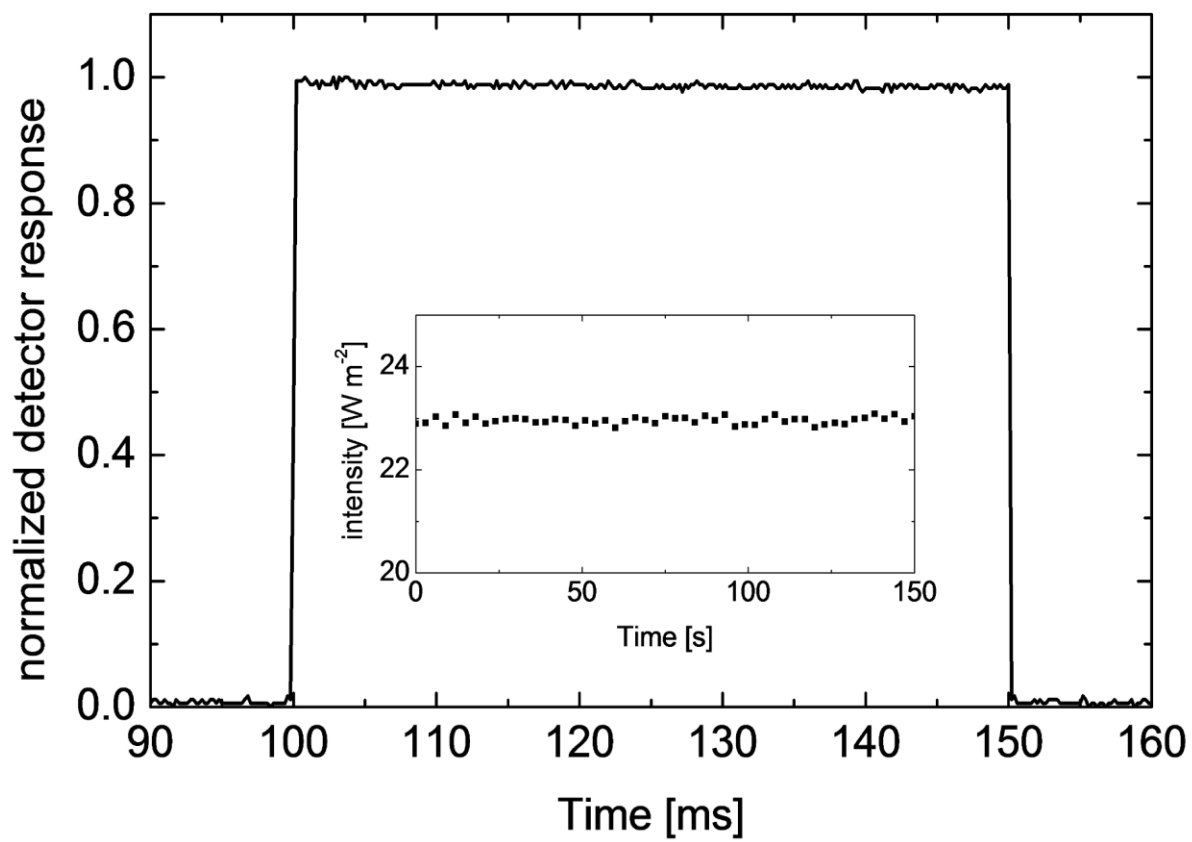


Figure 10

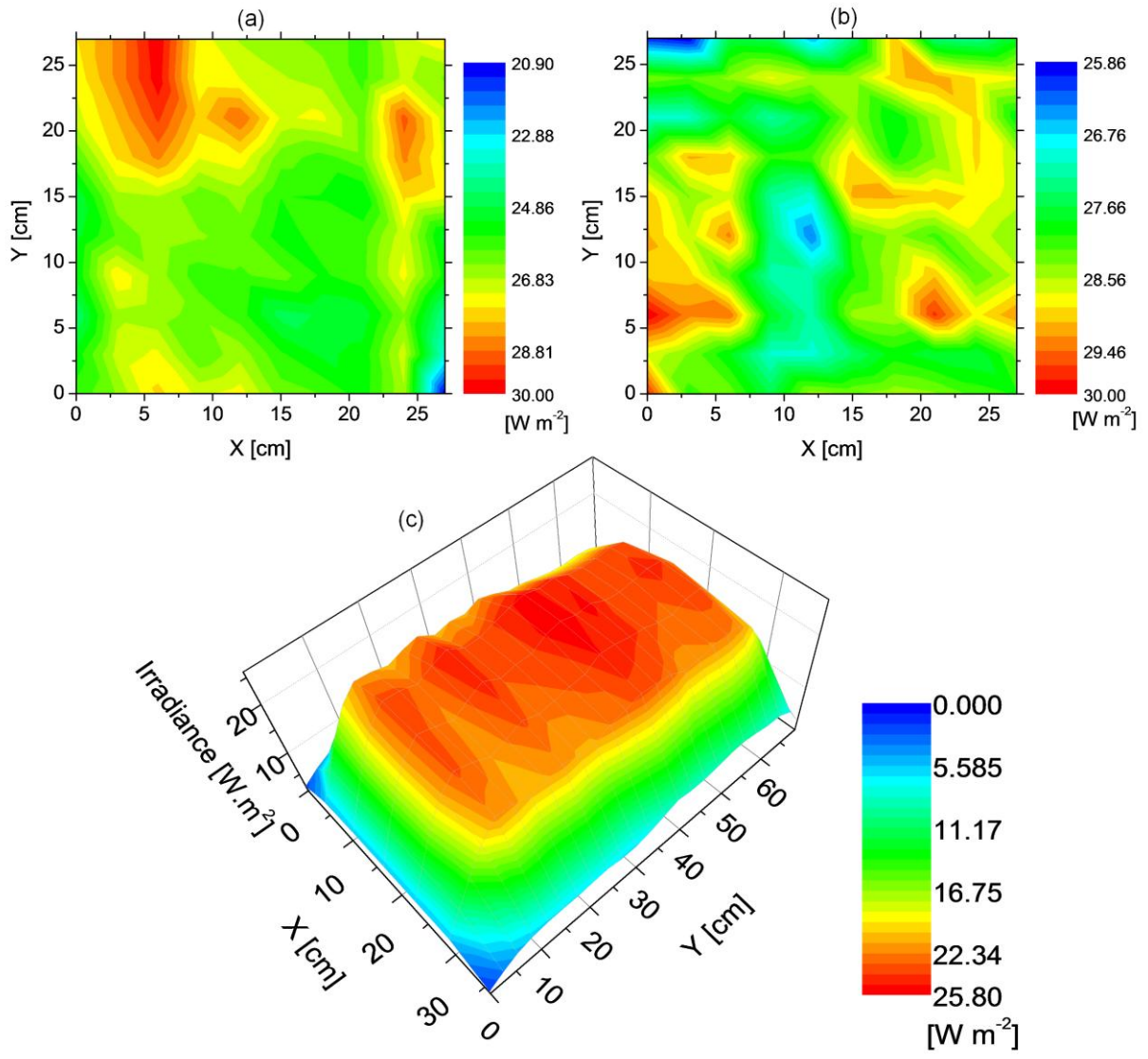


Figure 11

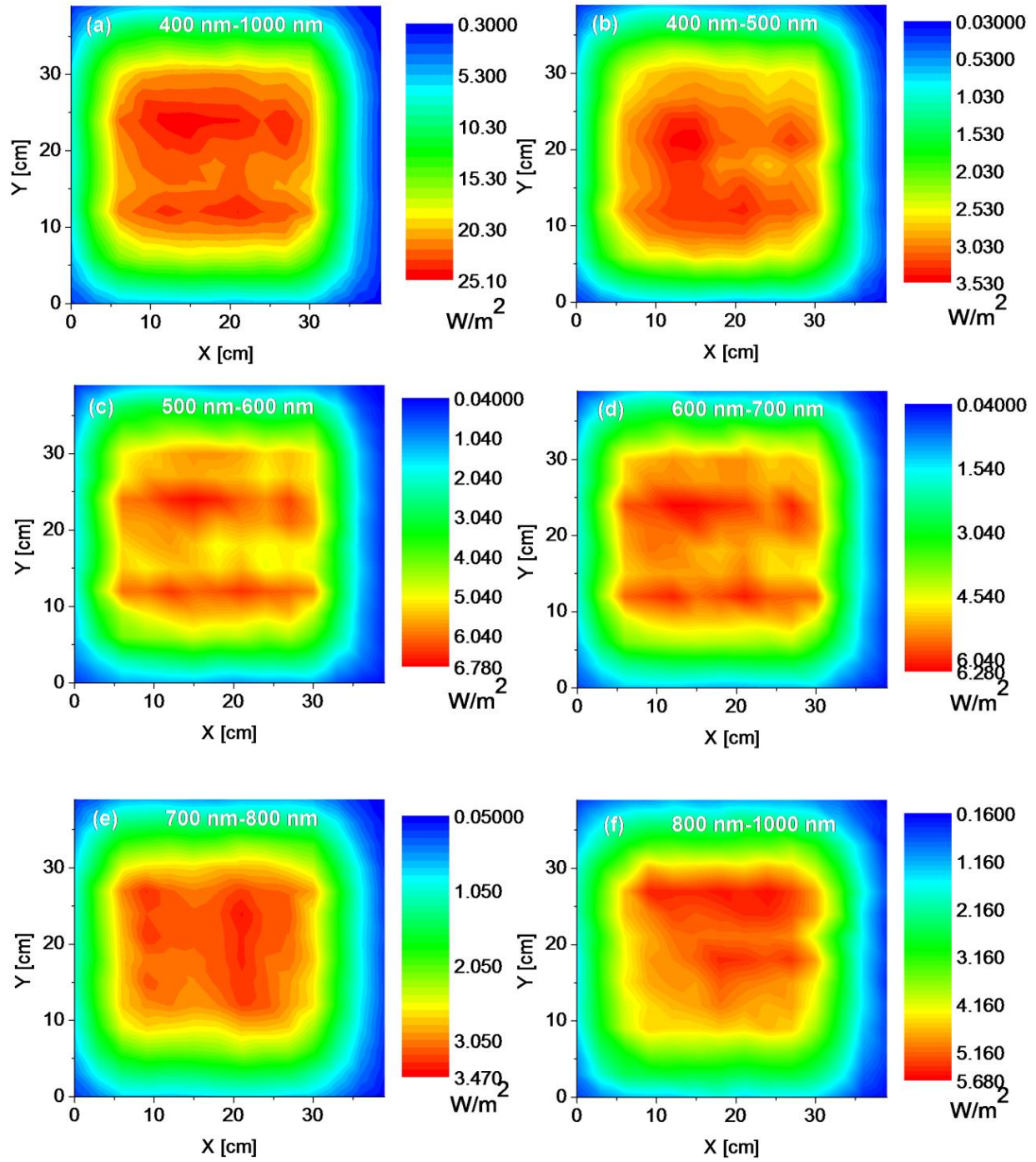


Figure 12